A New Form of the Polarimetric Notch Filter

Tao Liu, Ziyuan Yang, Tao Zhang, *Member*, *IEEE,* Yanlei Du, *Member*, *IEEE*, and Armando Marino, *Member*, *IEEE*

***Abstract*—Ship detection using polarimetric synthetic radar (PolSAR) imagery attracts lots of attention in recent years. Most notably, the detector polarimetric notch filter (PNF) has been demonstrated to be effective for ship detection in PolSAR imagery, which gives excellent performances. In this work a mathematical form of one new PNF (NPNF) based on physical mechanisms of targets and clutter is further developed for partial targets. The different mechanisms have been revealed based on the projection matrix. The experimental results including simulated data and measured data demonstrate that the NPNF exhibits a better performance than the original PNF.**

***Index Terms*—Polarimetry, Ship Detection, Synthetic Aperture Radar, Polarimetric Notch Filter**

I. Introduction

Synthetic aperture radar (SAR) is a common tool for ship detection. SAR has the ability to monitor ships during both day and night and under cloud cover [1]. A common way to perform detection is setting a statistical test on the intensity of the SAR image. This generally separated the brighter ships from the darker sea clutter. The tests are generally focused on the clutter distribution and the probability of false alarm (Pfa). In particular, the threshold is selected to keep the Pfa constant [i.e., the constant false-alarm rate (CFAR)] [1]-[4]. Considering the benefits of polarimetry in detecting and classifying targets in SAR images, it is not a surprise that many ship detectors use polarimetric SAR (PolSAR) to improve the performances of detecting small targets[1]–[6]. A relatively complete survey of techniques can be found in [5]. In summary, the detectors using polarization can be divided into five categories generally based on pixel detection: a) independent polarization channel composition, b) polarization optimization techniques, c) polarimetric scattering mechanism, d) ship wake detection and e) data driven or machine learning. And recently the patch detectors are presented to improve the detection performance, such as super-pixels segmentation based detectors. Recent advancements can be found in [6]. Among all the pixel based detectors the polarimetric notch filter (PNF) has been used for ship detection in polarimetric synthetic aperture radar (PolSAR) images and gives an excellent performance [1]. Its final expression is the following [1][2]

$$\gamma = \frac{1}{\sqrt{1+\dfrac{RedR}{\mathbf{t}^H\mathbf{t}-\left|\mathbf{t}^H\hat{\mathbf{t}}_{sea}\right|^2}}} = \frac{1}{\sqrt{1+\dfrac{RedR}{P_T}}} \tag{1}$$

where $RedR$ is the reduction ratio, $\mathbf{t}$ is the partial target feature vector, $\hat{\mathbf{t}}_{sea}$ is the normalized feature scattering factor of the sea clutter, $\hat{\mathbf{t}}_{sea}=\mathbf{t}_{sea}/\|\mathbf{t}_{sea}\|$ and $\|\cdot\|$ denotes the Euclid norm. H stands for conjugate transpose and γ is the polarimetric coherence operator.

In [1], it has been proven that a statistical detector set on Eq (1) has identical performance of a detector testing the following equation

$$P_T = \mathbf{t}^H\mathbf{t}-\left|\mathbf{t}^H\hat{\mathbf{t}}_{sea}\right|^2 \tag{2}$$

where P_T represents the power component of the target of interest. This is because there is a deterministic 1 to 1 transformation that leads Eq (2) to Eq (1).

In single target case (a single target is defined as a deterministic target), $\mathbf{t}$ is the polarimetric scattering vector, which is generally denoted as $\mathbf{k}=\begin{bmatrix} S_{hh} & \sqrt{2}S_{hv} & S_{vv}\end{bmatrix}^T$. S_{xy} represents the complex scattering coefficient with x as the transmitting and y is the receiving polarization (h-linear horizontal, v-linear vertical). T stands for transpose.

In the partial targets case (each pixel of such distributed targets may have a specific polarimetric behavior), $\mathbf{t}$ is the vector formed by the vectorization of the covariance matrix. $\mathbf{t}$ is defined as $\mathbf{t}=[c_{11}^{1/2}\ c_{22}^{1/2}\ c_{33}^{1/2}\ c_{12}^{1/2}\ c_{23}^{1/2}\ c_{13}^{1/2}]^T$, where c_{ij} are the elements of the covariance matrix $\mathbf{C}=\frac{1}{L}\sum_{i=1}^{L}\mathbf{k}_i\mathbf{k}_i^H=\left(c_{ij}\right)_{d\times d}$ $(1\le i,j\le d, d=3)$. L is the average number of looks. Here the Euclid norm is defined as $\|\mathbf{t}\|=\left(\sum_{i=1}^{6}|t_i|^2\right)^{1/2}$.

II. New Form of the Polarimetric Notch Filter

In the original version, the feature scattering factor is formed by the vectorization of the covariance matrix for partial targets [1][2]. The vectorization leads to a signal processing definition of power (squared length of the vector) and implies that the importance of each elements of the covariance matrix is identical when discriminating targets and clutter. In this different version, we propose to evaluate power with a definition that is closer to the physical scattered power from the target (i.e. Trace of the covariance matrix). To do this a new

[1] This work was supported in part by the National Natural Science Foundation of China under Project 61771483, 41822105, 61490693.

T. Liu and Z. Yang are with the school of electronic engineering, Naval University of Engineering, Wuhan, 430033, China (e-mail: liutao1018@hotmail.com).

T. Zhang and Y. Du are with the department of electronic engineering, Tsinghua University, Beijing, 100084, China.

A. Marino is with the Faculty of Natural Sciences, University of Stirling, UK (armando.marino@stir.ac.uk).

formulation of the PNF is proposed, where we move away from the original partial target formalism and consider targets in the scene as single targets. The target power in Eq (2) can be substituted in the single target case as follows

$$P_T = \mathbf{k}^H\mathbf{k} - \mathbf{k}^H\left(\hat{\mathbf{k}}_{sea}\hat{\mathbf{k}}_{sea}^H\right)\mathbf{k} = \mathbf{k}^H\mathbf{k} - \mathbf{k}^H\hat{\mathbf{C}}_{sea}\mathbf{k} = \mathbf{k}^H\left(\mathbf{I} - \hat{\mathbf{C}}_{sea}\right)\mathbf{k} \tag{3}$$

where $\mathbf{I}$ is the identity matrix, and $\hat{\mathbf{C}}_{sea} = \hat{\mathbf{k}}_{sea}\hat{\mathbf{k}}_{sea}^H$ is the normalized polarimetric covariance matrix. In partial targets case, by adding an averaging to reduce speckle, Eq (3) can be extended to

$$P_T = \frac{1}{L}\sum_{i=1}^{L}\mathbf{k}_i^H\left(\mathbf{I} - \hat{\mathbf{C}}_{sea}\right)\mathbf{k}_i = \mathrm{tr}\left(\left[\mathbf{I} - \hat{\mathbf{C}}_{sea}\right]\mathbf{C}\right) \tag{4}$$

where $\mathbf{C}$ is the measured covariance matrix. $\mathbf{C}$ can be estimated by the average of real data divided by the equivalent number of looks L. The normalized covariance matrix is obtained from the large and pure clutter region by $\hat{\mathbf{C}}_{sea} = \left\langle \hat{\mathbf{k}}_{sea}\hat{\mathbf{k}}_{sea}^H \right\rangle = \mathbf{C}_{sea} / \mathrm{tr}(\mathbf{C}_{sea})$. $\mathrm{tr}(\cdot)$ is the trace operator and $\langle\square\rangle$ is the average operator. Please note, the average is not applied to the full operator, but only the P_T component inside the PNF equation. It is therefore a new form of the detector which cannot be directly derived from the first one in Eq (3) without adding this step in Eq (4). This also means that the detection performance of a statistical test based on the new form is not bound to be the same as the original PNF.

Additionally, we do not need to consider the full form γ of the NPNF defined in Eq (1) where the coherence evaluation is performed and we can stick with Eq (4). For consistency, in the following comparisons we will also use the expression of the PNF based on P_T in Eq (2).

Finally, we want to double check that the two detectors provide independent information. For doing this, we simply plot the NPF against the NPNF over the entire AIRSAR dataset. The result plotted in Fig 1 show that the two are independent.

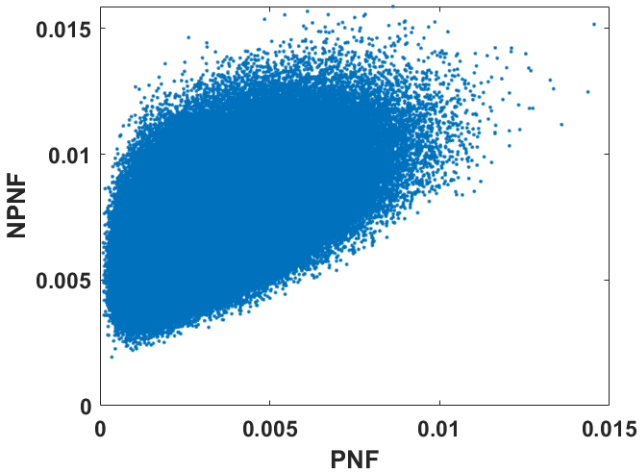

Fig 1 The relation curve of PNF and NPNF

Interesting $\left(\mathbf{I} - \hat{\mathbf{C}}_{sea}\right)$ is an orthogonal projection matrix. From a mathematical point of view, we can see that the PNF for partial targets is a 6-dimensional projection, while the NPNF splits the space to three 3-dimensional sub-spaces and then sum the sub-space projection energy. Therefore they both consider the full space of polarimetric target, but the difference is in the weighting of the off diagonal elements. Appendix shows the extended mathematical expression with all coefficients. Another important point is to check that the NPNF is non-negative. Since $\hat{\mathbf{C}}_{sea}$ is the $d \times d$ positive semidefinite Hermite matrix (d is the dimension of the scattering vector), we can obtain the following equation according to the eigenvalue decomposition theorem:

$$\begin{aligned}\mathbf{I} - \hat{\mathbf{C}}_{sea} &= \mathbf{U}^H\mathbf{I}\mathbf{U} - \mathbf{U}^H\begin{bmatrix}\varsigma_1 & & & \\ & \varsigma_2 & & \\ & & \ddots & \\ & & & \varsigma_d\end{bmatrix}\mathbf{U} \\ &= \mathbf{U}^H\begin{bmatrix}1-\varsigma_1 & & & \\ & 1-\varsigma_2 & & \\ & & \ddots & \\ & & & 1-\varsigma_d\end{bmatrix}\mathbf{U}\end{aligned} \tag{5}$$

where $1 \ge \varsigma_1 \ge \varsigma_2 \ge \cdots \ge \varsigma_d \ge 0$, $\varsigma_j (j = 1,2,\cdots d)$ is the eigenvalue of $\hat{\mathbf{C}}_{sea}$ and $\mathbf{U}$ is a unitary matrix. $\mathbf{I} - \hat{\mathbf{C}}_{sea}$ is positive semidefinite because $\hat{\mathbf{C}}_{sea}$ is a normalized matrix and the sum of its eigenvalues is equal to 1. Therefore each of the diagonal elements in Eq (5) is bound to be non-negative.

It can be found that both $\mathbf{I} - \hat{\mathbf{C}}_{sea}$ and $\mathbf{C}$ are positive semidefinite. There exists a matrix trace inequalities for product of positive semidefinite matrices [7]

$$0 \le \mathrm{tr}(\mathbf{AB}) \le \mathrm{tr}(\mathbf{A})\mathrm{tr}(\mathbf{B}) \tag{6}$$

This ensures the result in Eq (4) to be nonnegative. It should also be noted that Eq (4) can used for both the data formats of the single look complex (SLC) and multilook complex (MLC).

III. Validation

In this section, simulated and real data are used to validate the performance of the NPNF. We also compare the results with the original PNF method. The flowchart of the NPNF detector is presented in Fig 2.

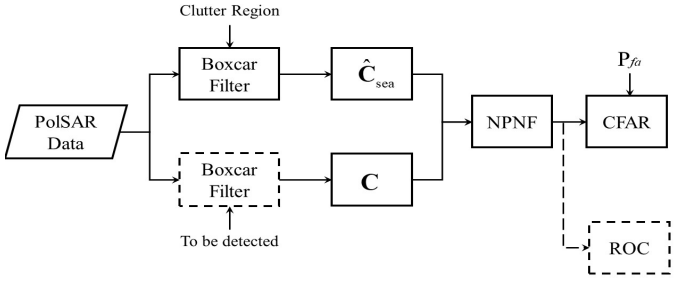

Fig 2 Flowchart of the NPNF detector

The solid parallelograms represent the input. The solid rectangular boxes show the operation and procedure the boxcar filter is used to estimate the polarimetric covariance matrices for both clutter and targets to be detected. The "Pfa" is the probability of false alarm, and the "ROC" is the Receiver

Operating Characteristics. The dotted rectangular box is optional, which can be operated to accelerate the detection speed or to assess the performances of different detectors.

A) Simulated Data Validation: We used Wishart distribution to characterize the statistical variation of covariance matrix of clutter. We understand that this is restrictive since the sea has been proven to have a substantial texture component; however this allows us to do some benchmarking based on some Monte Carlo (MC) simulations. The targets are generally not distributed as Wishart, and we assume they obey G0-Wishart distribution, where the texture obeys unitary inverse gamma distribution [4]. The asymptotic covariance matrices used in the MC were selected from real AIRSAR data (which are described in details in Section B).

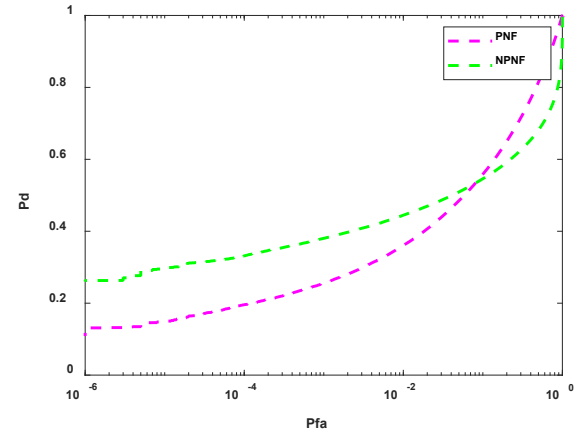

(b) TCR=1

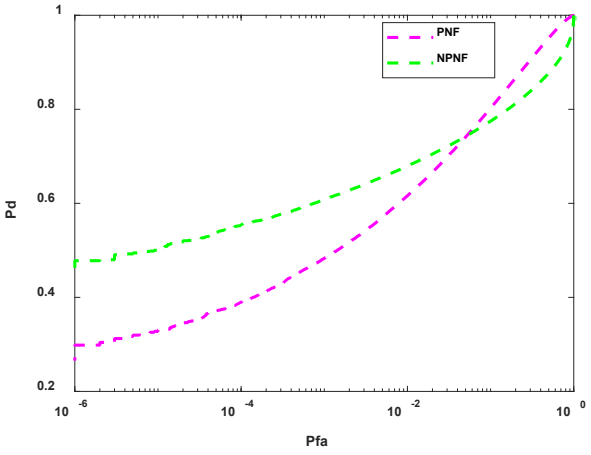

(c) TCR=2

Fig 3 Comparisons in the case of Wishart model for clutter and G0-Wishart for targets with different TCRs

The synthetic MC data set consists of N =1,000,000 covariance matrix samples drawn from a complex, circular, and zero-mean Wishart distribution. In G0-Wishart model the unitary textual variables of clutter are generated according to the shape parameter λ=2 , while the shape parameters is 4 for targets. The number of looks was set to $L = 9$ .The ROC curves are shown in Fig 3. In the following figures, "TCR" is the target to clutter ratio, and "Pd" is the probability of detection. The target to clutter ratio (TCR) is defined as [7]

$$TCR = \mathrm{tr}(\boldsymbol{\Sigma}_T - \boldsymbol{\Sigma}_C) / \mathrm{tr}(\boldsymbol{\Sigma}_C) \quad (7)$$

where $\boldsymbol{\Sigma}_T$, $\boldsymbol{\Sigma}_C$ are the estimated polarimetric covariance matrices of targets and clutter respectively.

But if the statistical characteristics are very heterogeneous for the clutter and ships, there is little difference between PNF and NPNF and the detection performance descends. The results are presented in Fig 4 and Fig 5, which are in agreement with those for the Wishart case. We see that the performance of NPNF is better when the TCR gets larger.

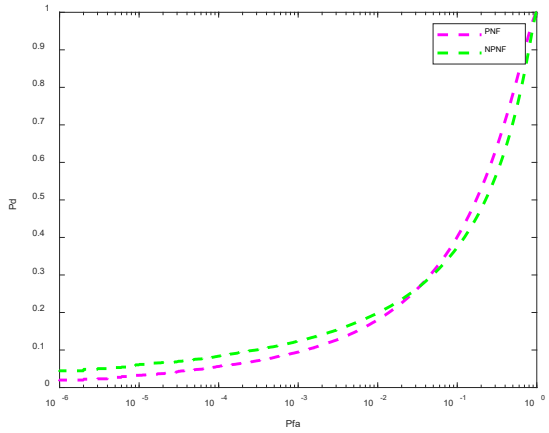

Fig 4 Comparisons in the case of a K-Wishart model for clutter and a G0-Wishart model for targets (TCR=1)

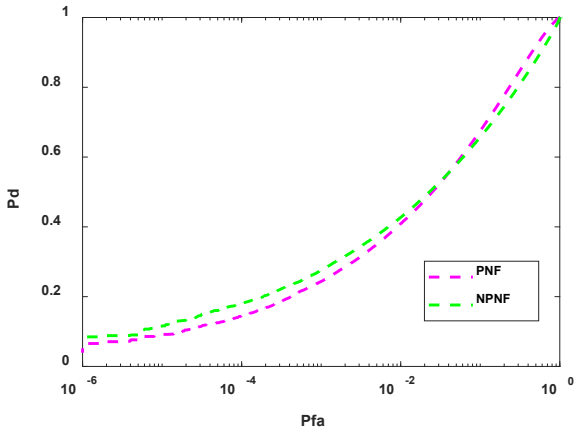

Fig 5 Comparisons in the case of a G0-Wishart model for clutter and a G0-Wishart model for targets (TCR=1)

B) Measured Data Validation: Two polarimetric SAR datasets are used. One real data is a 9-look NASA/JPL AIRSAR polarimetric dataset that covers the Japanese inland sea named Kojimawan near Tamano City [9]. The dataset is fully polarimetric and acquired on October 4, 2000 by the AIRSAR instrument during the PACRIM-2 mission. The same region of interest (ROI) is selected as that in [9] where the ground truth is known. The ROI is presented in Fig 6, where there are 22 ships identified by S1~S22.

To assess the performance of the CFAR detectors we consider: 1) the false alarm rate maintenance, 2) the figure of merit (FOM) and 3) the ROC curves. The CFAR loss C_L is a function dependent on the threshold and indicates the

corresponding error between the actual PFA $\overline{P}_{fa}$ and PFA $\hat{P}_{fa}$ estimated by the model, which is defined as [4]

$$C_L = \left| 20\log\left(\overline{P}_{fa} / \hat{P}_{fa} \right) \right| \tag{8}$$

The FOM is a more suitable index for performance evaluation. FOM is defined as in [9]

$$FoM = \frac{N_{td}}{\left(N_{fa} + N_{gt} \right)} \tag{9}$$

where N_{td} is the number of detected targets, N_{fa} is the number of false alarms, N_{gt} is the total number of targets actually present.

The ROC is plotted to assess the detection performance of the different detectors. A big difference in the estimation of FOM is that we consider each pixel of the vessel as a target pixel. Since we don't have a very large amount of ships, to make the curves smoother, we picked most of the ship pixels as targets from visual inspection, which is also adopted in [10]. Therefore the ROC curves are estimates of the performance in delineating ships additionally to detecting them.

A CFAR framework called fast block CFAR is used [11]. The region of interest (ROI) is divided into equally sized blocks and then the brightest pixels are removed before estimation.

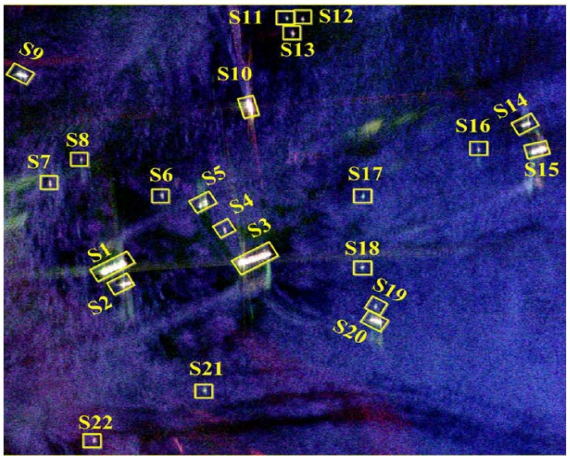

Fig 6 The ground-true data provided by AIRSAR

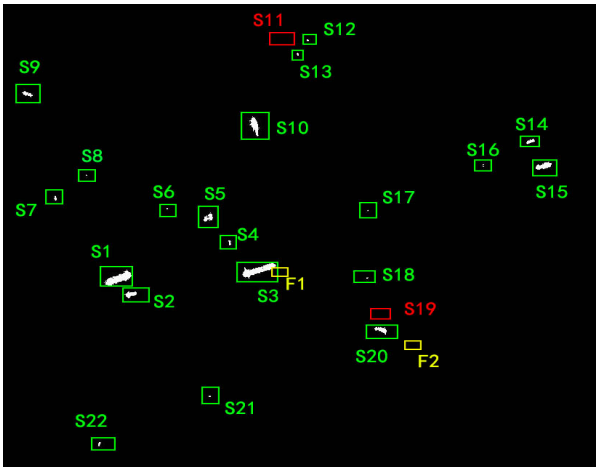

(a) PNF

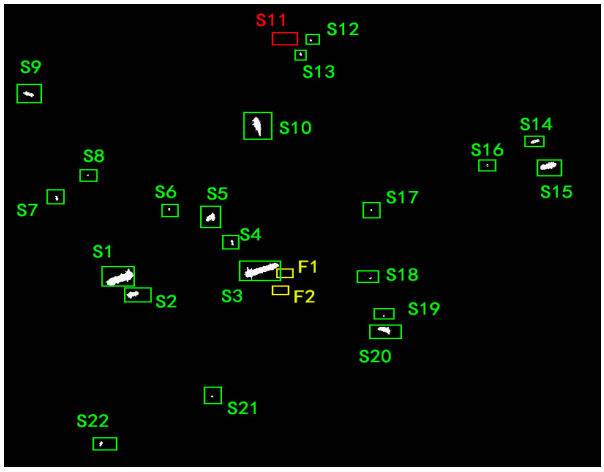

(b) NPNF

Fig 7 the results of different polarimetric detectors

Here the block size is 256 x 256, and the threshold to remove ships is 0.15 dealing with the PNF output. Though there are still some ship pixels used to estimate the clutter statistics, they can be ignored for they are extremely fewer compared with the sea clutter pixels. The detection results are presented in Fig 7, where a red rectangle means an omitted target, a yellow rectangle means a false target, and a green rectangle means one true ship. The CFAR loss and the FOM are shown in table 1 when the actual PFA is set 1e-5, and the generalized gamma distribution (GΓD) is used to model the PNF and the NPNF. The parameter estimation is based on log-cumulants [4][11]. The ROC curves are also shown in Fig 8. The result from the ROC curves is in agreement with that from the FOM. The NPNF gives better performance according to both the FOM and ROC curves.

TABLE 1 PERFORMANCES OF BOTH DETECTORS IN AIRSAR IMAGERY

ROI	Method	N_{td}	N_{fa}	C_L	$FoM(\%)$
AIRSAR	PNF	20	2	9.54	83.33
	NPNF	21	2	9.54	87.50

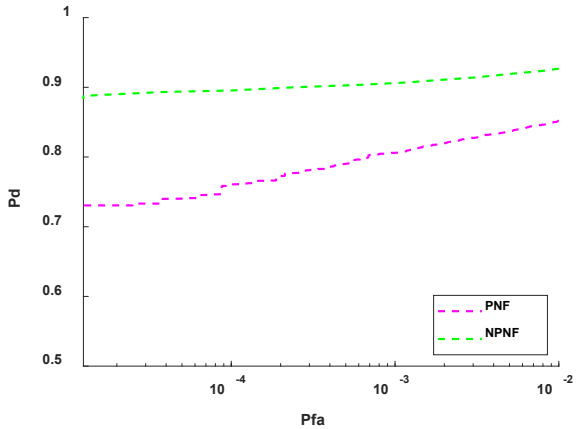

Fig 8 The ROC curves of the detection results in AIRSAR data

The second dataset is a UAVSAR L-Band fully polarimetric

image. Its corresponding Pauli RGB image is shown in Fig. 9, where 71 ships are totally presented. More details on this dataset can be found in [10]. In [10], the PNF reaches the best detection performance based on the ROC assessment. The performance comparison by ROC curves for the UAVSAR image is shown in Fig 10 and other detection results are omitted due to page limitation. The obtained results are consistent with those carried out on simulation data. The reason why the detection performances of PNF and NPNF are different may be that the cross components may contain more noisy information and therefore when the TCR is low, neglecting them in the formalism of the PNF may improve the performance.

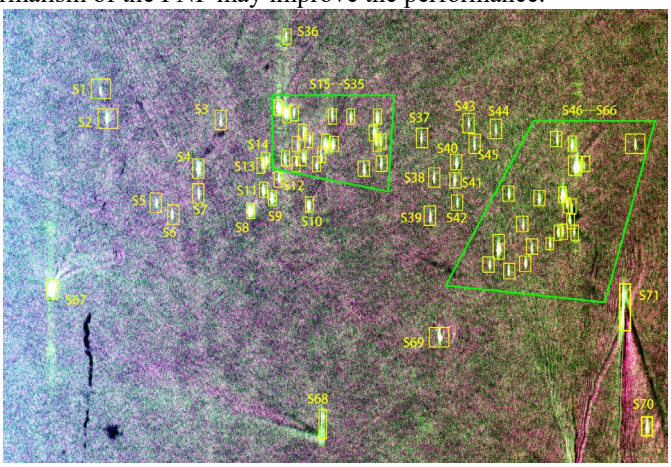

Fig 9 The ground-true data of the ROI provided by UAVSAR

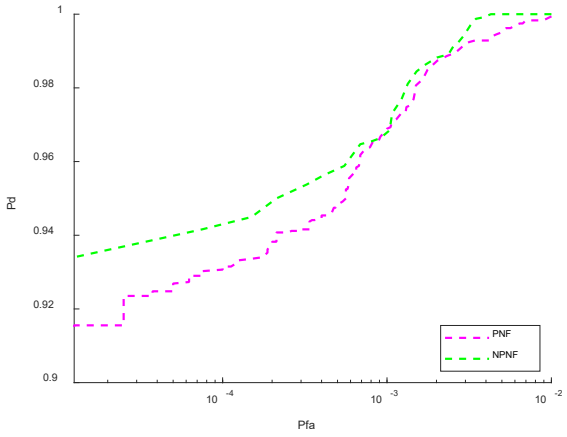

Fig 10 The ROC curves of the detection results in UAVSAR imagery

IV. Conclusion

Instead of using the vectorization of the covariance matrix, a new form of the PNF (NPNF) has been proposed based on the single target vectors. The experiments demonstrated that NPNF can provide better performance than the existing PNF.

Appendix

To describe the difference between the two forms of the PNF, the expanded expressions are presented here. The covariance matrices are denoted as follows:

$$\mathbf{C}=\left(c_{ij}\right)_{d\times d},\ \mathbf{C}_{sea}=\left(c_{sea\_ij}\right)_{d\times d},1\le i,j\le d \tag{A.1}$$

d is the dimension of the matrix, which equals 3 generally. The final forms of the PNF and NPNF are presented.

$$\begin{aligned}P_{T-PNF}&=\mathbf{t}^H\mathbf{t}-\left|\mathbf{t}^H\hat{\mathbf{t}}_{sea}\right|^2\\&=c_{11}+c_{22}+c_{33}+|c_{12}|+|c_{13}|+|c_{23}|\\&\quad-\frac{\left|\left(c_{11}^{1/2}\right)^H c_{sea\_11}^{1/2}+\left(c_{22}^{1/2}\right)^H c_{sea\_22}^{1/2}+\left(c_{33}^{1/2}\right)^H c_{sea\_33}^{1/2}+\left(c_{12}^{1/2}\right)^H c_{sea\_12}^{1/2}+\left(c_{13}^{1/2}\right)^H c_{sea\_13}^{1/2}+\left(c_{23}^{1/2}\right)^H c_{sea\_23}\right|^2}{c_{sea\_11}+c_{sea\_22}+c_{sea\_33}+|c_{sea\_12}|+|c_{sea\_13}|+|c_{sea\_23}|}\end{aligned} \tag{A.2}$$

$$\begin{aligned}P_{T-NPNF}&=\frac{1}{c_{sea\_11}+c_{sea\_22}+c_{sea\_33}}\times\\&\left[c_{11}(c_{sea\_11}+c_{sea\_22})+c_{22}(c_{sea\_11}+c_{sea\_33})+c_{33}(c_{sea\_11}+c_{sea\_22})\right.\\&\left.-2\,\mathrm{Re}(c_{12}c_{sea\_12}^H)-2\,\mathrm{Re}(c_{13}c_{sea\_13}^H)-2\,\mathrm{Re}(c_{23}c_{sea\_23}^H)\right]\end{aligned} \tag{A.3}$$

where Re(·) means the real part of a complex value. We can see there is no obvious relation between the NPNF and the original PNF.

Reference

[1] A. Marino, "A Notch Filter for Ship Detection With Polarimetric SAR Data," in IEEE Journal of Selected Topics in Applied Earth Observations and Remote Sensing, vol. 6, no. 3, pp. 1219-1232, June 2013, doi: 10.1109/JSTARS.2013.2247741.

[2] A. Marino and I. Hajnsek, "Statistical Tests for a Ship Detector Based on the Polarimetric Notch Filter," in IEEE Transactions on Geoscience and Remote Sensing, vol. 53, no. 8, pp. 4578-4595, Aug. 2015.

[3] T. Zhang, Z. Yang, H. Gan, D. Xiang, S. Zhu and J. Yang, "PolSAR Ship Detection Using the Joint Polarimetric Information," in IEEE Transactions on Geoscience and Remote Sensing, doi: 10.1109/TGRS.2020.2989425.

[4] T. Liu, J. Zhang, G. Gao, J. Yang and A. Marino, "CFAR Ship Detection in Polarimetric Synthetic Aperture Radar Images Based on Whitening Filter," in IEEE Transactions on Geoscience and Remote Sensing. doi: 10.1109/TGRS.2019.2931353

[5] D. J. Crisp, "The state-of-the-art in ship detection in synthetic aperture radar imagery," DSTO, Dept. Defence, Canberra, Australia, Tech. Rep. DSTO-RR-0272, 2004

[6] X. Cui, Y. Su and S. Chen, "A Saliency Detector for Polarimetric SAR Ship Detection Using Similarity Test," in IEEE Journal of Selected Topics in Applied Earth Observations and Remote Sensing, vol. 12, n no. 9, pp. 3423-3433, Sept. 2019

[7] X. Yang, X. Yang, and K. L. Teo, "A matrix trace inequality," J. Math.Anal. Appl., vol. 263, pp. 327–333, 2001.

[8] L. M. Novak, M. B. Sechtin and M. J. Cardullo, "Studies of target detection algorithms that use polarimetric radar data," in IEEE Transactions on Aerospace and Electronic Systems, vol. 25, no. 2, pp. 150-165, March 1989.

[9] Wei J J, Li P X, and Yang J. et al., "A new automatic ship detection method using L-band polarimetric SAR imagery," IEEE Journal of Selected Topics in Applied Earth Observations and Remote Sensing, vol. 7, no. 4, pp. 1383-1393, Jul. 2014.

[10] Tao Zhang, Linfeng Jiang, Deliang Xiang, Yifang Ban, Ling Pei, Huilin Xiong, Ship detection from PolSAR imagery using the ambiguity removal polarimetric notch filter, ISPRS Journal of Photogrammetry and Remote Sensing, Volume 157, pp. 41-58, 2019.

[11] T. Liu, Z. Yang, A. Marino, G. Gao, and J. Yang, " Robust CFAR Detector Based on Truncated Statistics for Polarimetric Synthetic Aperture Radar," in IEEE Transactions on Geoscience and Remote Sensing. doi: 10.1109/TGRS.2020.2979252